

LA-UR-15-21831 (Accepted Manuscript)

Testing Actinide Fission Yield Treatment in CINDER90 for use in MCNP6 Burnup Calculations

Fensin, Michael Lorne
Umbel, Marissa

Provided by the author(s) and the Los Alamos National Laboratory (0000-00-00).

To be published in: Progress in Nuclear Energy, Volume 85, November 2015, Pages 719-728.

DOI to publisher's version: 10.1016/j.pnucene.2015.09.001

Permalink to record: <http://permalink.lanl.gov/object/view?what=info:lanl-repo/lareport/LA-UR-15-21831>

Disclaimer:

Approved for public release. Los Alamos National Laboratory, an affirmative action/equal opportunity employer, is operated by the Los Alamos National Security, LLC for the National Nuclear Security Administration of the U.S. Department of Energy under contract DE-AC52-06NA25396. Los Alamos National Laboratory strongly supports academic freedom and a researcher's right to publish; as an institution, however, the Laboratory does not endorse the viewpoint of a publication or guarantee its technical correctness.

1 Testing Actinide Fission Yield Treatment in CINDER90 for use in MCNP6 Burnup Calculations

2
3 M. L. Fensin (corresponding author) and Marissa Umbel
4 Los Alamos National Laboratory
5 MS C921
6 Los Alamos, NM 87545
7 +1 505 606 0145
8 *mfensin@lanl.gov*
9

10 Abstract

11
12 Most of the development of the MCNPX/6 burnup capability focused on features that were applied to the
13 Boltzman transport or used to prepare coefficients for use in CINDER90, with little change to CINDER90
14 or the CINDER90 data. Though a scheme exists for best solving the coupled Boltzman and Bateman
15 equations, the most significant approximation is that the employed nuclear data are correct and
16 complete. The CINDER90 library file contains 60 different actinide fission yields encompassing 36
17 fissionable actinides (thermal, fast, high energy and spontaneous fission). Fission reaction data exists for
18 more than 60 actinides and as a result, fission yield data must be approximated for actinides that do not
19 possess fission yield information. Several types of approximations are used for estimating fission yields
20 for actinides which do not possess explicit fission yield data. The objective of this study is to test whether
21 or not certain approximations of fission yield selection have any impact on predictability of major actinides
22 and fission products. Further we assess which other fission products, available in MCNP6 Tier 3, result in
23 the largest difference in production. Because the CINDER90 library file is in ASCII format and therefore
24 easily amendable, we assess reasons for choosing, as well as compare actinide and major fission product
25 prediction for the H. B. Robinson benchmark for, three separate fission yield selection methods: (1) the
26 current CINDER90 library file method (Base); (2) the element method (Element); and (3) the isobar method
27 (Isobar). Results show that the three methods tested result in similar prediction of major actinides, Tc-99
28 and Cs-137; however, certain fission products resulted in significantly different production depending on
29 the method of choice.

30
31 Highlights

- 32
- 33 • Examining fission yield data provides methodology for selecting an appropriate fission yield for
34 actinides not explicitly possessing fission yield data.
 - 35 • Based on fission yield data examination, the nearest element or nearest isobar seem to be
36 reasonable approximations for selecting a fission yield for an actinide not explicitly possessing
37 fission yield data.
 - 38 • Results show that the three methods tested result in similar prediction of major actinides, Tc-99
39 and Cs-137; however, certain fission products result in significantly different production
40 depending on the method of choice.

41
42 Keywords

43
44 MCNP6, CINDER90, Fission Yield, Burnup
45
46

47 1. Introduction

48

49 The first MCNP based inline Monte Carlo depletion capability was released as MCNPX 2.6.0 [1]. This
50 technology used MCNPX for solving the spatially dependent Boltzman equation (using the Monte Carlo
51 method) in order to provide destruction and creation coefficients and normalization constants for
52 CINDER90 [2] for solving the time dependent Bateman equations. Several features were developed in
53 order to model typical reactor calculations, and the genesis of each feature as well as comparisons of the
54 code's predictive capabilities to the H. B. Robinson fuel assembly benchmark were given in Ref 3. With
55 the later development of MCNP6 [4], simulation capabilities of MCNPX and MCNP5 were now integrated
56 into a single radiation transport code. The new MCNP6 burnup capability, using a new parallel
57 architecture, memory management scheme and improved physics, was later presented in 2014 [5]. Most
58 of the focus of the development of the MCNPX/6 burnup capability focused on features that were applied
59 to the transport or preparation of the coefficients for use in CINDER90 (i.e. supplying continuous energy
60 integrated collision densities, 63-group fluxes and normalization coefficients), with little change to
61 CINDER90 or the CINDER90 data (the only exception was an adjustment made to the (n,γ) collision rate to
62 improve isomer branching).

63

64 The destruction and creation coefficients of the Bateman equations are composed of both decay and
65 absorption rates (fission and capture). Because the absorption rates depend upon the time dependent
66 flux, which depends upon the time dependent atom densities, the entire depletion process is nonlinear
67 and an approximation must be made to make the process solvable. The usual approximation is to solve
68 for the creation and destruction coefficients at a time step, using a Boltzman solver, and then send these
69 coefficients to a Bateman solver, where these coefficients are assumed constant, to progress the number
70 densities to a new time step, where the process then repeats. This approximation is reasonable if the
71 time step is not large "enough" such that the atom densities do not change "enough" to warrant a
72 "significant change" in the time dependent flux (hence allowing for an approximation of constant reaction
73 rate over a time step). Because power is proportional to the product of the flux and macroscopic fission
74 cross section, in order to maintain a constant power level over a time step, the flux must increase during
75 the time step to compensate for loss of fissionable material from burnup (this argument is complicated
76 by the buildup of absorbers and fission products as well as loss of possible burnable poisons and possible
77 breeder material). As a result, the flux can never be constant in a real reactor, but if the time step is small
78 "enough" then the flux can be assumed constant "enough". Because the depletion process involves
79 marching through a series of time steps, making the time steps small "enough" may involve too many
80 time step calculations for reasonable computation. As a result, flux averaging techniques are employed
81 to lengthen the size of a "reasonable" time step. [6-8] MCNP6 employs a midpoint predictor corrector
82 scheme. [9]

83

84 Though a scheme exists for best solving the coupled Boltzman and Bateman equations, the most
85 significant approximation is that the employed nuclear data are correct and complete. Nuclear data in
86 the context of the Boltzman equation are transport cross sections and secondary particle production
87 information such as supplied by the Evaluated Nuclear Data Files (ENDF) [10] or similar evaluations from
88 other countries [11-14]. Nuclear Data in the context of the Bateman solver also includes transport cross
89 sections but is further extended to decay constants, branching ratios and fission yields. Not every nuclide
90 has a significant enough cross section to contribute to reactivity to further affect the magnitude and shape
91 of the flux; therefore using a subset of nuclides, in the Boltzman solver, to compute the magnitude and
92 shape of the flux is a "reasonable enough" approximation. MCNP useable neutron transport cross
93 sections only exist for ~400 nuclides; unfortunately, over a thousand nuclides can be produced from a
94 fission system. Therefore at best MCNP can only currently use these ~400 nuclides to calculate a

95 magnitude and shape of the flux (without adopting a method for creating fission product lumps to
96 approximate the ~1000 other nuclides created during the fission process). The Bateman solver must have
97 some type of approximation for the destruction and creation coefficients of the nuclides that do not
98 possess transport cross sections. For CINDER90, 63-group cross sections, for many reaction types, exist
99 for thousands of nuclides (~1/3 of the nuclides in the library file), and the user must provide a 63-group
100 flux in order to energy integrate to a total collision rate for each reaction type. The 63 group cross sections
101 in the CINDER90 library file were computed from codes like GNASH [15] and EMPIRE [16]. The CINDER90
102 library file also contains 60 different actinide fission yields encompassing 36 fissionable actinides (thermal,
103 fast, high energy and spontaneous fission). The available fission yields are given in Table 1. Each actinide
104 fission yield set contains production information for 1325 fission products. The fission yield sets in the
105 CINDER90 library file are normalized to 2.0 fission products per fission event; therefore tertiary fission
106 product emissions are not considered in this library. These fission yields are the yield data from ENDF/B
107 VI.0 and the chronology of where these data originated can be found in Ref 17.

108
109 Fission reaction data exists for more than 60 actinides and as a result, fission yield data must be
110 approximated for actinides that do not possessed fission yield information. In CINDER90, missing fission
111 yield data is approximated by using the Pu-239 fast fission yield or by using the available fission yield for
112 another impinging energy (use the fast yield if there is no thermal fission yield). The idea behind using
113 the fast fission yield if the thermal yield does not exist is that the actinide probably possesses a threshold
114 below which there exists no (or extremely minimal) fission cross section. Because, for some codes, the
115 user must select a single library or average fission energy for selecting a fission yield to use, implementing
116 the fast yield assumes that any fission that was tallied in a transport code, for the particular actinide, was
117 actually caused by fast fission regardless of whether or not the average fission energy of the system was
118 thermal. In other codes like ORIGEN2 (ORIGEN2 possesses fission yield data for 9 actinides), the total
119 fission rate from all actinides without explicit fission product yields is calculated, and the actinide with the
120 largest fission contribution is used to select a nearest available neighbor yield; and then the fission product
121 yield of the nearest neighbor is adjusted to account for the total number of fissions from actinides that do
122 not have explicit yields [18]. In ORIGEN-S [19], the successor to ORIGEN2, fission yield data exists for 30
123 actinides; however, actinides without explicit yields do not produce fission products during fission.
124 ORIGEN-S does provide the ability to energy interpolate fission yields based on the average neutron
125 energy causing fission for each fissionable nuclide [20]. Other point depletion codes around the world
126 have their own methods for treating missing fission yields, which either leverage a substitution concept
127 (like CINDER90), a nearest neighbor approach like ORIGEN2 or not producing fission products at all for
128 nuclides lacking yields. [21-23]

129
130 The objective of this study is to test whether or not certain approximations of fission yield selection have
131 any impact on predictability of major actinides and fission products. The motivation of this work is
132 therefore to understand how these approximations ultimately affect the prediction of actinides given in
133 typical spent fuel benchmark analysis. Unfortunately, measurement of minor fission products is not
134 necessarily covered in typical spent fuel benchmark analysis. This gap in analysis is usually due to
135 abundance, cost and/or relative importance to predicting aspects of the spent fuel with these fission
136 products (there are better markers for burnup, enrichment, etc.). Therefore though this study does also
137 assess which other fission products, available in MCNP6 Tier 3 (Tier 3 is the most inclusive set of fission
138 products that are tracked during the transport calculation), result in the largest difference in production,
139 we only choose to report the difference as the main focus of the work is connected to the prediction of
140 major actinides and fission products found in typical spent fuel benchmark analysis.

141

142 One major advantage of the CINDER90 depletion package is that the CINDER90 library file is in ASCII text
 143 readable format; and therefore can be easily altered to test various nuclear data approximations. Fission
 144 yields that can be selected for a typical actinide are listed directly in the library file, and therefore can be
 145 easily manipulated. Unfortunately, for neutron induced fission, CINDER90 can only currently use either
 146 thermal, fast or high energy fission yields without further energy interpolation (a set of yields is pre-
 147 selected). Modifying the CINDER90 code to interpolate yield information is not within the scope of this
 148 study. Given that we cannot energy interpolate fission yields in CINDER90, we leverage the ASCII format
 149 of the library file to compare, using the H. B. Robinson Benchmark, three strategies for selecting fission
 150 product yields for actinides not explicitly containing fission yield data: (1) selecting the Pu-239 fast fission
 151 yield or an available fast yield (default in CINDER90); (2) choosing the nearest neighbor element yield; and
 152 (3) selecting the nearest available isobar yield. The H. B. Robinson reactor is a thermal reactor and hence
 153 for this study we only test thermal fission yield choices for actinides used in CINDER90.

154
 155 Table 1. Available CINDER90 fission product yield sets.

Actinide	Thermal	Fast	HE	SF
Th-227	x			
Th-229	x			
Th-232		x	x	
Pa-231		x		
U-232	x			
U-233	x	x	x	
U-234		x	x	
U-235	x	x	x	
U-236		x	x	
U-237		x		
U-238		x	x	x
Np-237	x	x	x	
Np-238		x		
Pu-238		x		
Pu-239	x	x	x	
Pu-240	x	x	x	
Pu-241	x	x		
Pu-242	x	x	x	
Am-241	x	x	x	
Am-242m	x			
Am-243		x		
Cm-242		x		
Cm-243	x	x		
Cm-244		x		x
Cm-245	x			
Cm-246		x		x
Cm-248		x		x
Cf-249	x			
Cf-250				x

Cf-251	x	
Cf-252		x
Es-253		x
Es-254	x	
Fm-254		x
Fm-255	x	
Fm-256		x

157

158

159 2. Theory

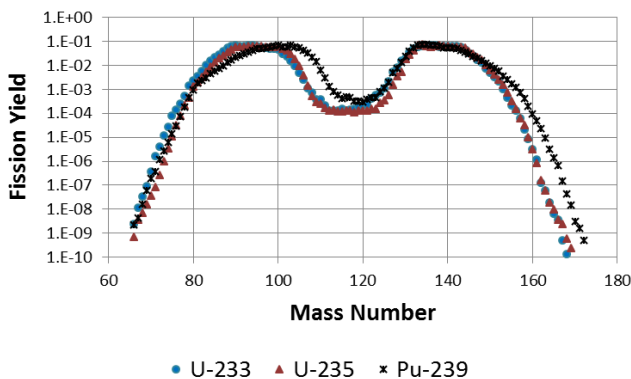
160

161 Though the existence of positively charged protons would seem to break apart the nucleus through
 162 electrostatic repulsion, the short range strong nuclear force dominates and holds the nucleus in a near
 163 spherical configuration. When 6-8 MeV is supplied to the nucleus (either by binding energy of a neutron
 164 or kinetic energy from a particle), the spherical shape is perturbed to an ellipse and then oscillates into an
 165 “eight shape” (if considering binary fission). When the separation in the “eight shape” is past a critical
 166 range, the electrostatic repulsion between the fragments dominates, and the nucleus fissions. The fission
 167 of any actinide has a distribution of probable fission product pairs (if only considering binary fission),
 168 where the distribution for a particular target actinide depends upon the energy of the incoming neutron
 169 as well as the mass of the target actinide.

170

171 Figure 1 displays the normalized fission product chain yields of U-233, U-235 and Pu-239, for thermal
 172 induced fission, where the yield of each isobar is summed for a particular mass number (as taken from
 173 the CINDER90 library file). For thermal fission, the fission yield curve has a double hump shape, where
 174 the double hump is shifted towards the higher mass if the mass of target actinide is greater. Shifting from
 175 U-233 to U-235 represents a mass percent increase of only 0.86% while shifting from U-235 to Pu-239
 176 represents a mass increase of 1.7%. When we visually inspect the curves it seems that the shift from U-
 177 233 to U-235 is not half as large as the shift from U-235 to Pu-239; therefore one could hypothesize that
 178 yields within an element may have similar structure.

179



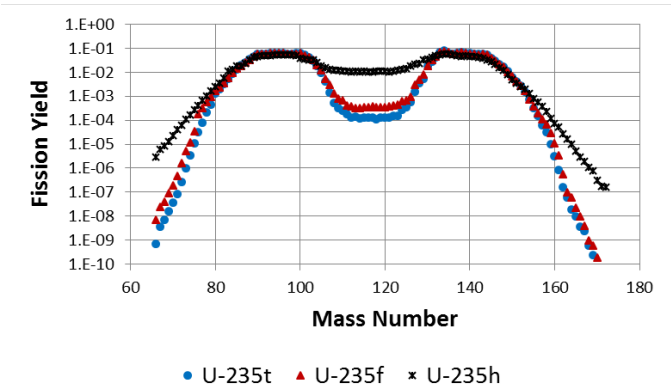
180

181 Figure 1. Normalized fission product yield of U-233, U-235 and Pu-239 thermal fission.

182

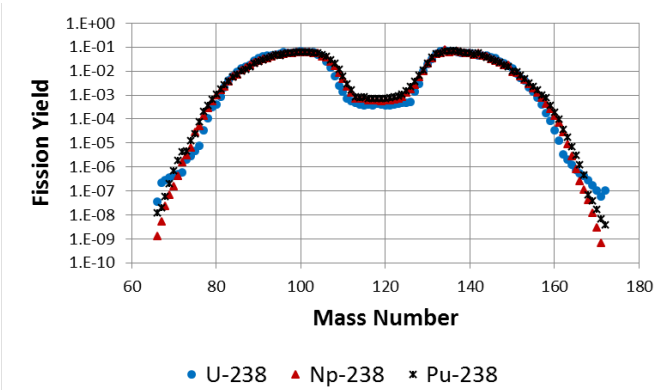
183 Figure 2 displays the normalized fission product chain yields for thermal, fast and high energy induced
 184 fission of U-235 (“t” designates a thermal fission yield; “f” designates a fast fission yield; “h” designates a
 185 high energy fission yield). As the impinging neutron energy increases, the dip in the center of the double

186 hump is raised creating a more uniform probability of sampling a fission product within the double hump
 187 range in a given fission event; however, between a thermal induced fission and a fast induced fission, the
 188 raise in the dip is not as large as going from fast induced fission to high energy induced fission. In fact, for
 189 $A=115$, the increase in thermal to fast fission yield is 1.69 times larger, while going from fast to high energy
 190 fission, the increase is 31.22 times larger.
 191
 192



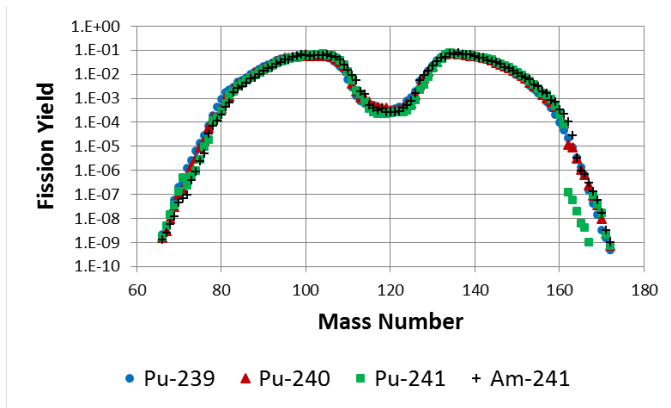
193
 194 Figure 2. Normalized fission product yield for thermal, fast and high energy induced fission of U-235.
 195

196 Figure 3 displays the normalized fission product chain yields for fast induced fission of U-238, Np-238 and
 197 Pu-238. These particular fission chain yields were chosen because these targets share the common isobar
 198 of $A=238$. Excluding the tails of the fission yield distribution, the fission product yields, summed over each
 199 isobar line up on top of each other. Figure 4 displays normalized fission product chain yields for thermal
 200 induced fission of Pu-239, Pu-240, Pu-241 and Am-241. With the exception of Pu-241's greater than
 201 $A=160$ wing, the distributions also lie almost on top of each other. Figure 5 displays ratios of the fission
 202 yields for various common isobars and various common elements. For fission products of mass number
 203 "A", where $80 < A < 160$, both methods look reasonable. Examining particularly $105 < A < 130$, we see that the
 204 isobar method for $A=238$ fast fission has a slightly larger ratio than for the listed element thermal fission
 205 yields of plutonium; however, Am-241 thermal fission yield slightly better predicts Pu-241 thermal fission
 206 than the other listed Pu isotopes for certain fission product mass numbers. Therefore, from these
 207 particular comparisons, we can only conclude that the common isobar and common element methods
 208 both look like reasonable approximations for fission yields that are not explicitly given; however, we
 209 cannot yet conclude that one method is better than the other in terms of effect on a calculated results.
 210



211
 212 Figure 3. Normalized fission product yields for fast induced fission of U-238, Np-238 and Pu-238.

213

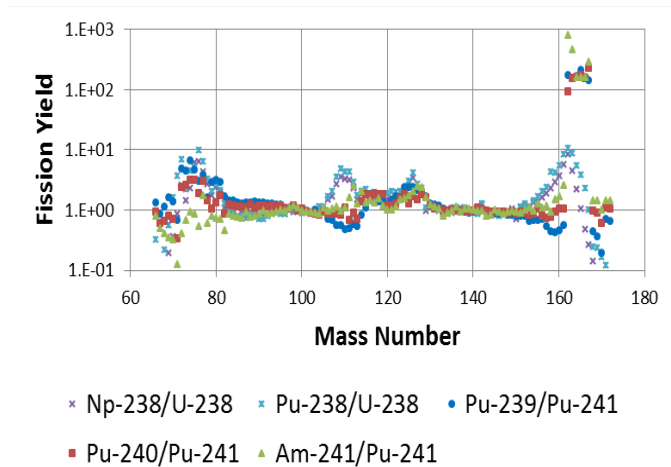


214

215 Figure 4. Normalized fission product yields for thermal induced fission of Pu-239, Pu-240, Pu-241 and Am-241.

216

217

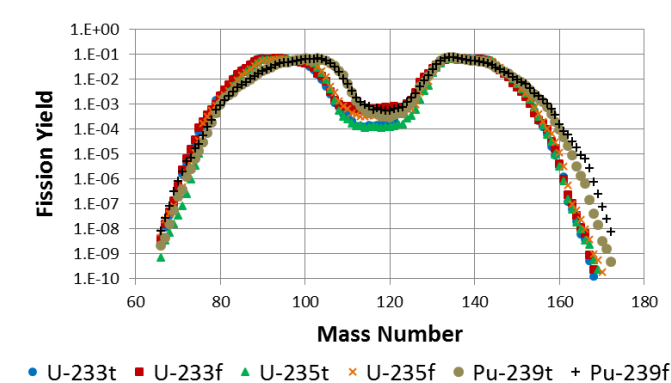


218

219 Figure 5. Fission product yield ratios for A=238 fast fission and Pu-239, Pu-240, Pu-241 and Am-241 thermal fission.

220

221



222

223 Figure 6. Normalized fission product chain yields for thermal and fast induced fission of U-233, U-235 and Pu-239.

224

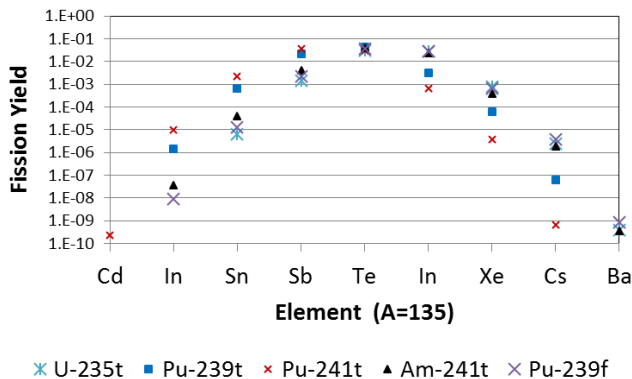
225

226 Figure 6 displays normalized fission product chain yields for thermal and fast induced fission of U-233, U-235 and Pu-239. Figure 6 seems to show that selecting a fission yield within a common element of the

227

228 same induced energy is better than selecting the yield of the same isotope at a different induced energy.
 229 The arguments made for Figure 2, regarding the raise in the dip between the double humps of the mass
 230 chain yield curve with increasing impinging neutron energy, further support this hypothesis. When
 231 moving to a much higher mass number and different element, choosing the yield of the same isotope with
 232 different induced energy is better than choosing the yield of a different element, with lower mass number,
 233 at the same induced energy; this phenomenon is evident from the shift in the mass chain yield curve to
 234 the right when comparing U-235 thermal fission to Pu-239 thermal fission. Though the dip between the
 235 double humps of the mass chain yield curve is raised going from Pu-239 thermal to Pu-239 fast fission,
 236 the shift right in mass chain yield from U-235 thermal fission to Pu-239 thermal fission is more
 237 pronounced. Figures 6 also demonstrates that blindly choosing Pu-239 fast fission yield for every fission
 238 yield not explicitly given by ENDF/B VI.0 is probably not the best approximation.
 239

240 Figure 7 shows the distribution of yields of fission products A=135 for U-235, Pu-239, Pu-241 and Am-241
 241 thermal fission yields and Pu-239 fast fission yield (metastable yields are excluded for simplicity). A=135
 242 is chosen because Xe-135 is one of the larger reactivity contributors, and hence affects nuclides whose
 243 production is dictated by the shape and magnitude of the thermal flux. The yield distributions between
 244 isobars (PU-241/Am-241) do not behave as similar as the yield distributions amongst an element (Pu-
 245 239/Pu-241); however, Pu-239 fast fission yield does seem to match Am-241 thermal yield better than
 246 Pu-241 thermal yield. Therefore isobar summed fission mass chain yield plots can be a bit misleading as
 247 summing over the isobar does mask independent yield (yield of a single isotope) information.
 248



249
 250 Figure 7. Distribution of yields of fission products A=135 for Pu-239, Pu-241 and Am-241 thermal fission
 251 yields and Pu-239 fast fission yield (metastable yields are excluded for simplicity).
 252

253 The evidence above does suggests that a fission product yield selection method, for actinides not explicitly
 254 containing a fission product yield, that is based on either nearest available element or available isobar
 255 should improve prediction capability by providing a reasonable enough distribution of fission products.
 256 However, will such a new fission yield selection method actually have any impact on actinide/ major fission
 257 product prediction? Is one method better than another?
 258

259 3. Method

260
 261 For each fissionable species in the CINDER90 library file, the fission yield to use for thermal, fast and high
 262 energy fission is given by the line "B, C, D = (n,f) yield sets" for each fissionable actinide in the data file;
 263 where B, C and D are numbers associated with the fission yield. To associate a number with a particular
 264 target and energy, the user can search on the word "Fission" in the CINDER90 library file; and then the

265 user will be taken to a table associating each fission yield with a number (these numbers are used to
266 populate B, C and D for each fissionable actinide in the CINDER90 library file). We test three separate
267 fission yield selection methods: (1) the current CINDER90 library file method (Base); (2) the element
268 method (Element); and (3) the isobar method (Isobar).

269
270 The Base method uses the Pu-239 fast fission yield for all actinides not explicitly containing fission yield
271 data, except if a fission yield exists for another energy. For example, if the fast fission yield exists and the
272 thermal fission yield does not, then the fast fission yield is selected for thermal fission.

273
274 The Element method uses the explicit thermal fission yield if the respective explicit thermal fission yield
275 is given; otherwise, the yield is altered by: (1) selecting element A+1 (where A is the mass number), and if
276 the explicit thermal fission yield exists, then it is used; (2) if no explicit thermal fission yield is given for A+1,
277 then A-1 is selected and if the explicit thermal fission yield exists, then it is used; and/or (3) the procedure
278 is repeated with (A+n) and (A-n) (where n starts as n=2 and is incremented as n=n+1) until the nearest
279 explicit thermal fission yield is reached (if no explicit thermal fission yield exists but a fast fission yield
280 exists, then the closest explicit fast fission yield is used). For example, since Pa-233 thermal fission yield
281 does not exist, then A+1 is searched. Since Pa-234 explicit thermal fission yield does not exist, A-1 is
282 searched, and the process is repeated for (A+n) and (A-n) until a Pa explicit thermal fission yield is
283 identified. Since no Pa isotope has an explicit thermal fission yield, Pa-231 fast yield is selected for Pa-233
284 thermal fission yield.

285
286 The Isobar method also uses the actual yield if given; otherwise, if no explicit yield is present then either:
287 (1) the isobar line is followed by looking at Z+1, and then Z-1 and if needed (Z+n) and (Z-n) (where n starts
288 as n=2 and is incremented as n=n+1) until a fission yield is found; or (2) if an actinide with a fission yield
289 on the isobar line does not exist, then if the element is below Th-227, use Th-227 for thermal fission yields;
290 otherwise, if the element is above Th-227, then first look at A+1 and A-1, and then go up one element as
291 well as going down one element and look for the nearest yield by going to A+1 and A-1. For example,
292 since Np-234 thermal fission yield does not exist, A=234 isobars are searched. Since no A=234 isobars
293 contain an explicit thermal fission yield, A=235 isobars are searched; and because U-235, which is an
294 isobar of Np-235, contains an explicit fission yield, U-235 thermal fission yield is used for Np-234 thermal
295 fission yield. Tables 2a-b contain the thermal fission yield choices for each of the three tested methods.

296
297

298 Table 2a. Thermal fission yield selection for each method.

Actinide	Base	Element	Isobar
Rn-222	Pu-239f	Th-227t	Th-227t
Ra-223	Pu-239f	Th-227t	Th-227t
Ra-224	Pu-239f	Th-227t	Th-227t
Ra-225	Pu-239f	Th-227t	Th-227t
Ac-225	Pu-239f	Th-227t	Th-227t
Ra-226	Pu-239f	Th-227t	Th-227t
Ac-226	Pu-239f	Th-227t	Th-227t
Ac-227	Pu-239f	Th-227t	Th-227t
Th-227	Th-227t	Th-227t	Th-227t
Ra-228	Pu-239f	Th-227t	Th-229t
Th-228	Pu-239f	Th-229t	Th-229t
Pa-228	Pu-239f	Pa-231f	Th-229t
Th-229	Th-229t	Th-229t	Th-229t
Pa-229	Pu-239f	Pa-231f	Th-229t
Th-230	Pu-239f	Th-229t	Th-229t
Pa-230	Pu-239f	Pa-231f	Th-229t
U-230	Pu-239f	U-232t	Th-229t
Th-231	Pu-239f	Th-232t	U-232t
Pa-231	Pa-231f	Pa-231f	U-232t
U-231	Pu-239f	U-232t	U-232t
Th-232	Th-232f	Th-229t	U-232t
Pa-232	Pu-239f	Pa-231f	U-232t
U-232	U-232t	U-232t	U-232t
Pa-233	Pu-239f	Pa-231f	U-233t
U-233	U-233t	U-233t	U-233t
Th-234	Pu-239f	Th-229t	U-235t
U-234	U-234f	U-235t	U-235t
Np-234	Pu-239f	Np-237t	U-235t
U-235	U-235t	U-235t	U-235t
Np-235	Pu-239f	Np-237t	U-235t
U-236	U-236f	U-235t	Np-237t
Np-236	Pu-239f	Np-237t	Np-237t
Pu-236	Pu-239f	Pu-239t	Np-237t
U-237	U-237f	U-235t	Np-237t
Np-237	Np-237t	Np-237t	Np-237t
Pu-237	Pu-239f	Pu-239t	Np-237t

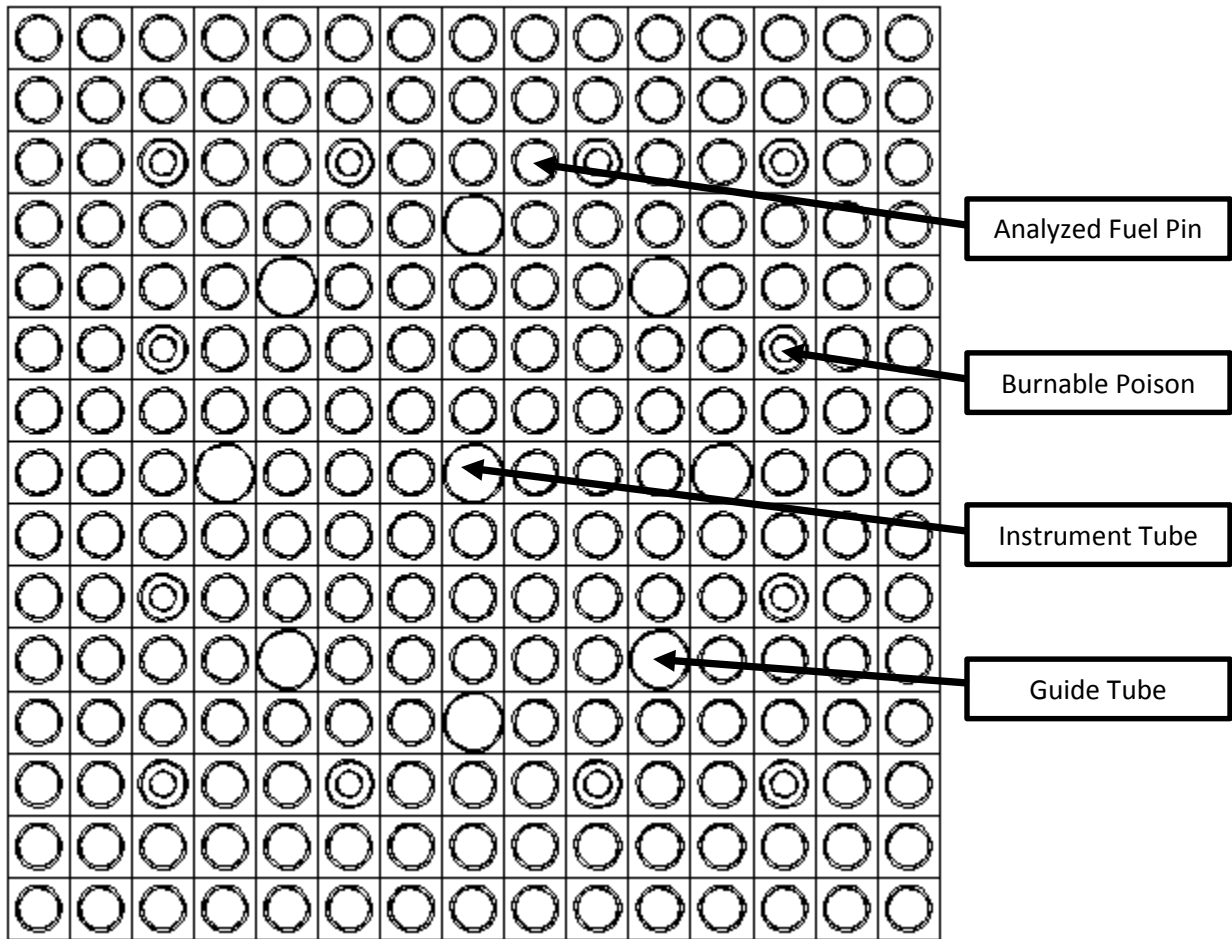
299
300 Table 2b. Thermal fission yield selection for each method.

Actinide	Base	Element	Isobar
U-238	U-238f	U-235t	Np-237t

Np-238	Np-238f	Np-237t	Pu-239t
Pu-238	Pu-238f	Pu-239-t	Pu-239t
Np-239	Pu-239f	Np-237t	Pu-239t
Pu-239	Pu-239t	Pu-239t	Pu-239t
Pu-240	Pu-240t	Pu-240t	Pu-240t
Am-240	Pu-239f	Am-241t	Pu-240t
Cm-240	Pu-239f	Cm-243t	Pu-240t
Pu-241	Pu-241t	Pu-241t	Pu-241t
Am-241	Am-241t	Am-241t	Am-241t
Cm-241	Pu-239f	Cm-243t	Am-241t
Pu-242	Pu-242t	Pu-242t	Pu-242t
Am-242	Pu-239f	Am-242mt	Am-242mt
Am-242m	Am-242mt	Am-242mt	Am-242mt
Cm-242	Cm-242f	Cm-243t	Am-242mt
Pu-243	Pu-239f	Pu-242t	Cm-243t
Am-243	Am-243f	Am-242mt	Cm-243t
Cm-243	Cm-243t	Cm-243t	Cm-243t
Pu-244	Pu-239f	Pu-242t	Cm-245t
Cm-244	Cm-244f	Cm-245t	Cm-245t
Cm-245	Cm-245t	Cm-245t	Cm-245t
Pu-246	Pu-239f	Pu-242t	Cm-245t
Cm-246	Cm-246f	Cm-245t	Cm-245t
Cm-247	Cm-242s	Cm-245t	Cf-249t
Cm-248	Cm-248f	Cm-245t	Cf-249t
Bk-249	Pu-239f	Cm-245t	Cf-249t
Cf-249	CF-249t	CF-249t	CF-249t
Cf-250	Pu-239f	Cf-251t	Cf-251t
Cf-251	Cf-251t	Cf-251t	Cf-251t
Cf-252	Pu-239f	Cf-251t	Cf-251t
Cf-253	Pu-239f	Cf-251t	Es-254t

301
302 To test the accuracy of these fission yield choices in an actual burnup calculation, the H. B. Robinson
303 burnup benchmark was simulated. The geometry and specifications used for benchmark were taken from
304 Ref 24. The setup (i.e. time steps, boundary conditions, etc.) was taken from Ref 3 and Ref 5, with the
305 two exceptions: (1) the kcode particles per cycle were increased to reduce relative error of the reaction
306 rates (10,000 particles per cycle skipping 25 cycles for a total of 130 active cycles); and (2) the S(a,b)
307 kernels were interpolated to the exact water temperature using the makssf utility [25]. The benchmark
308 is an infinitely reflected 15 by 15 UO₂ fueled, Zircaloy-4 clad subcooled fuel assembly. Figure 8 displays
309 an axial slice of the infinitely reflected fuel assembly. Table 3 lists the various parameters for setting up
310 the geometry. Table 4 details the average moderator temperature and density as well as average fuel
311 temperature. The benchmark provided results for four different burnups: 16.02 GWD/MTU, 23.8
312 GWD/MTU, 28.47 GWD/MTU and 31.66 GWD/MTU. Table 5 lists the parameters used for setting up the
313 burnup calculation. Because this benchmark only reported 2 fission products, this test served only to
314 understand the reactivity effect associated with a specific yield choice (as well as accuracy in prediction

315 of Cs-137 and Tc-99) for an actinide not specifically possessing an explicit yield. This benchmark was
 316 chosen because: (1) a model with reasonable MCNP6 predictive capability already existed; and (2) there
 317 existed no complications with modelling Gd burnout, control rod motion and/or boundary conditions due
 318 to shuffling sequence, which can be extremely complex to model and therefore complicate gauging the
 319 effect of the new yield choice.
 320



321
 322 Figure 8. Axial slice of the infinitely reflected H. B. Robinson fuel assembly geometry.
 323

324 Table 3. Fuel assembly design data for the H. B. Robinson benchmark*.

Parameter	Data
Assembly general data	
Designer	Westinghouse
Lattice	15 × 15
Number of fuel rods	204
Number of guide tubes	8
Number of burnable poison rods	12
Number of instrument tubes	1
Assembly pitch	21.50 cm

Assembly fuel	443.7 kg U
Fuel rod data	
Type of fuel pellet	UO ₂
Enrichment: wt % U-235	2.561
wt % U-234	0.023
wt % U-236	0.013
Pellet density	9.944 g/cc
Rod Pitch	1.43 cm
Rod OD	1.0719 cm
Rod ID	0.9484 cm
Pellet diameter	0.9242 cm
Active fuel length	365.76 cm
Clad temperature	595 K
Clad material	Zircaloy-4
Guide tube data	
Inner radius	0.6502 cm
Outer radius	0.6934 cm
Material	Zircaloy-4
Instrument tube data	
Inner radius	0.6502 cm
Outer radius	0.6934 cm
Material	Zircaloy-4
Burnable poison rod data	
Air OD	0.5677 cm
SS304 OD	0.6007 cm
Air OD	0.6172 cm
Borosilicate glass OD	1.0058 cm
Air OD	1.0173 cm
SS304 OD	1.1151 cm

325 *Data taken from Ref 24.

326

327 Table 4. Average temperature and moderator density for H. B. Robinson fuel assembly.

Burnup [GWD/MTU]	Moderator Temperature [K]	Moderator Density [g/cc]	Fuel Temperature [K]
16.02	559	0.7544	743
23.81	559	0.7538	830
28.47	576	0.7208	883
31.66	579	0.7135	923

328

329

330

331 Table 5. Burnup calculation setup for H. B. Robinson fuel assembly.

Parameter	Cycle			
	1	2	3	4
Operating interval [days]	243.5	243.5	156	156
Interval time step	1, 15, 20, 30,	1, 15, 20, 30,	1, 15,	1, 15, 20,
Durations [days]	37, 44, 46, 50.5	37, 44, 46, 50.5	20, 30, 40, 50	30, 40, 50*
Downtime [days]	40	64	39	--**
Average soluble boron concentration [ppm]	625.5	247.5	652.5	247.5

332 * This value was set to 59 for the 16.02 GWD/MTU case.

333 ** This value was set either to 3936 for the 16.02 and 23.8 GWD/MTU cases or 3637 for the 28.47
334 GWD/MTU and 31.66 GWD/MTU cases.

335

336 4. Results

337

338 Each benchmark calculation was run with the same cross section set as given in Ref 3 and Ref 5 (excluding
339 the exceptions given in the Methods section). This benchmark provided isotopic information for U-235,
340 U-236, U-238, Np-237, Pu-238, Pu-239, Pu-240, Pu-241, Tc-99 and Cs-137. Table 6-9 display the mass
341 percent difference $[100*(C/E-1)]$ for each burnup. The prediction of the actinides and two major fission
342 products, provided by the benchmark, for all 3 methods deviated less than a fraction of a percent from
343 between each method at each burnup. At 16.02, 23.08 and 31.66 GWD/MTU, the uranium isotopes are
344 a little bit better predicted by the element method; however, at 16.02 GWD/MTU, the plutonium isotopes,
345 Np-237 and Tc-99 are not better predicted by the element method. MCNP6 burnup does not propagate
346 errors in the atom density predictions; however, the errors in the reaction rates are printed at the end of
347 each step. For these calculations, the errors of any particular reaction rate did not exceed 5% (for most
348 reactions of most isotopes the error in reaction rate was less than 3%).

349

350 Table 6. H. B. Robinson results at 16.02 GWD/MTU.

Isotope	16.02 GWD/MTU		
	Base	Element	Isobar
U-235	3.16	3.12	3.21
U-236	-3.33	-3.29	-3.40
U-238	0.06	0.06	0.06
Pu-238	-3.71	-4.43	-4.27
Pu-239	8.79	9.12	9.29
Pu-240	0.81	1.18	1.87
Pu-241	4.88	4.63	3.75
Np-237	-2.64	-3.19	-3.13
Tc-99	8.39	8.49	9.05
Cs-137	-3.10	-2.90	-2.96

351 Mass percent difference $[100*(C/E-1)]$

352

353

354 Table 7. H. B. Robinson results at 23.8 GWD/MTU.

23.8 GWD/MTU			
Isotope	Base	Element	Isobar
U-235	3.07	2.86	2.93
U-236	-2.82	-2.62	-2.81
U-238	-0.60	-0.60	-0.60
Pu-238	-5.10	-5.68	-5.53
Pu-239	6.90	6.46	6.71
Pu-240	1.53	0.74	1.38
Pu-241	2.93	3.13	3.13
Np-237	-5.23	-5.79	-5.07
Tc-99	5.58	5.51	6.14
Cs-137	-3.01	-2.82	-2.82

355 Mass percent difference [100*(C/E-1)]

356

357 Table 8. H. B. Robinson results at 28.7 GWD/MTU.

28.47 GWD/MTU			
Isotope	Base	Element	Isobar
U-235	-4.50	-4.59	-4.42
U-236	2.20	2.22	2.11
U-238	0.47	0.47	0.47
Pu-238	-12.55	-12.15	-12.10
Pu-239	1.94	1.52	1.76
Pu-240	1.91	1.55	1.29
Pu-241	-5.75	-5.60	-6.05
Np-237	2.43	2.78	3.13
Tc-99	11.62	11.45	12.18
Cs-137	0.19	0.35	0.27

358 Mass percent difference [100*(C/E-1)]

359

360 Table 9. H. B. Robinson results at 31.66 GWD/MTU.

31.66 GWD/MTU			
Isotope	Base	Element	Isobar
U-235	-1.26	-1.15	-1.20
U-236	0.19	0.10	0.02
U-238	-0.79	-0.79	-0.73
Pu-238	-8.04	-8.19	-8.04
Pu-239	2.40	2.23	2.17
Pu-240	1.34	1.65	0.41
Pu-241	-3.00	-2.86	-3.08
Np-237	2.96	3.02	3.72
Tc-99	8.19	8.19	8.74

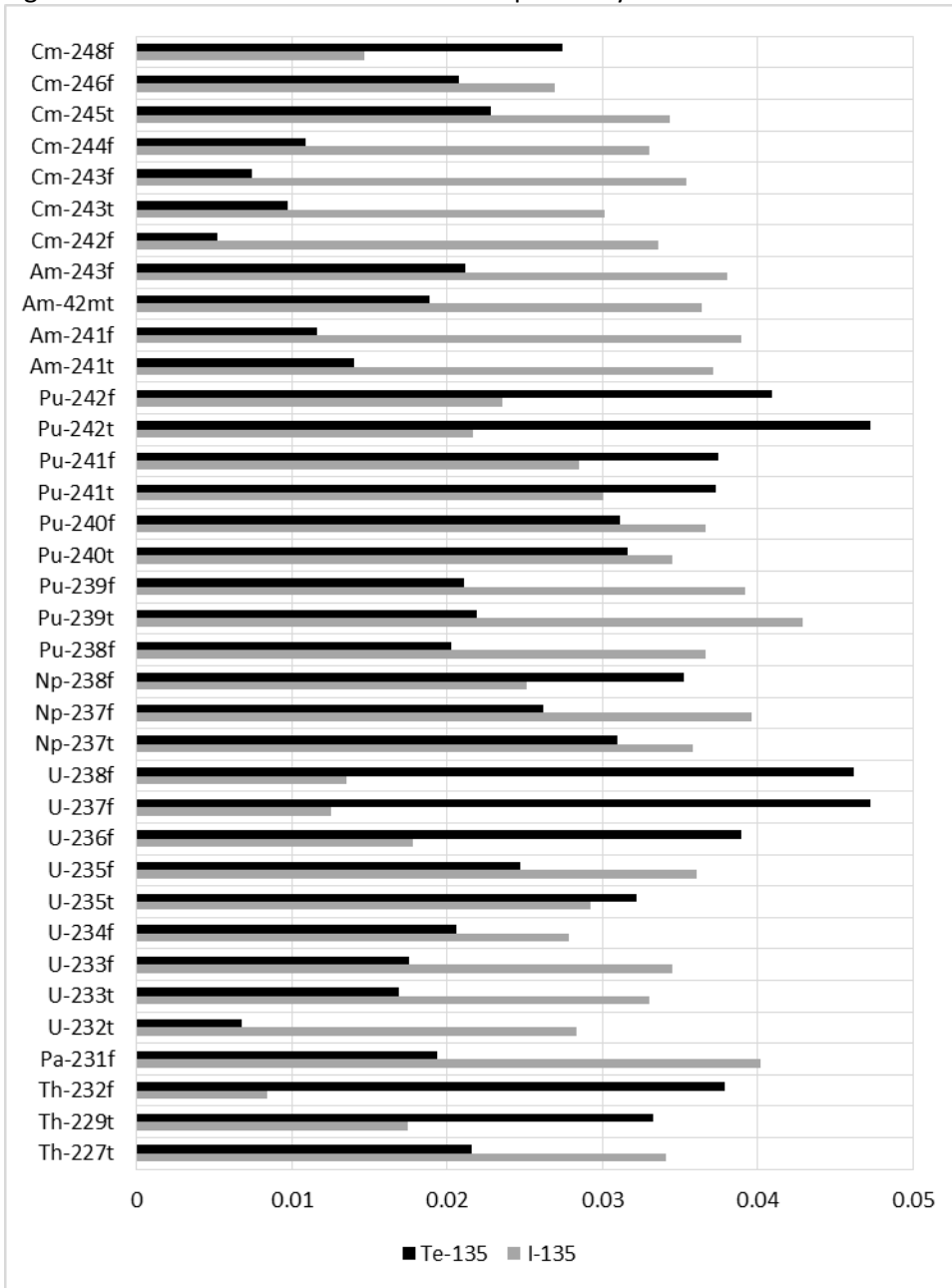
Cs-137 -2.16 -1.95 -2.09

Mass percent difference [100*(C/E-1)]

361
362
363
364
365
366
367
368
369
370
371
372
373
374
375
376
377
378
379
380
381
382

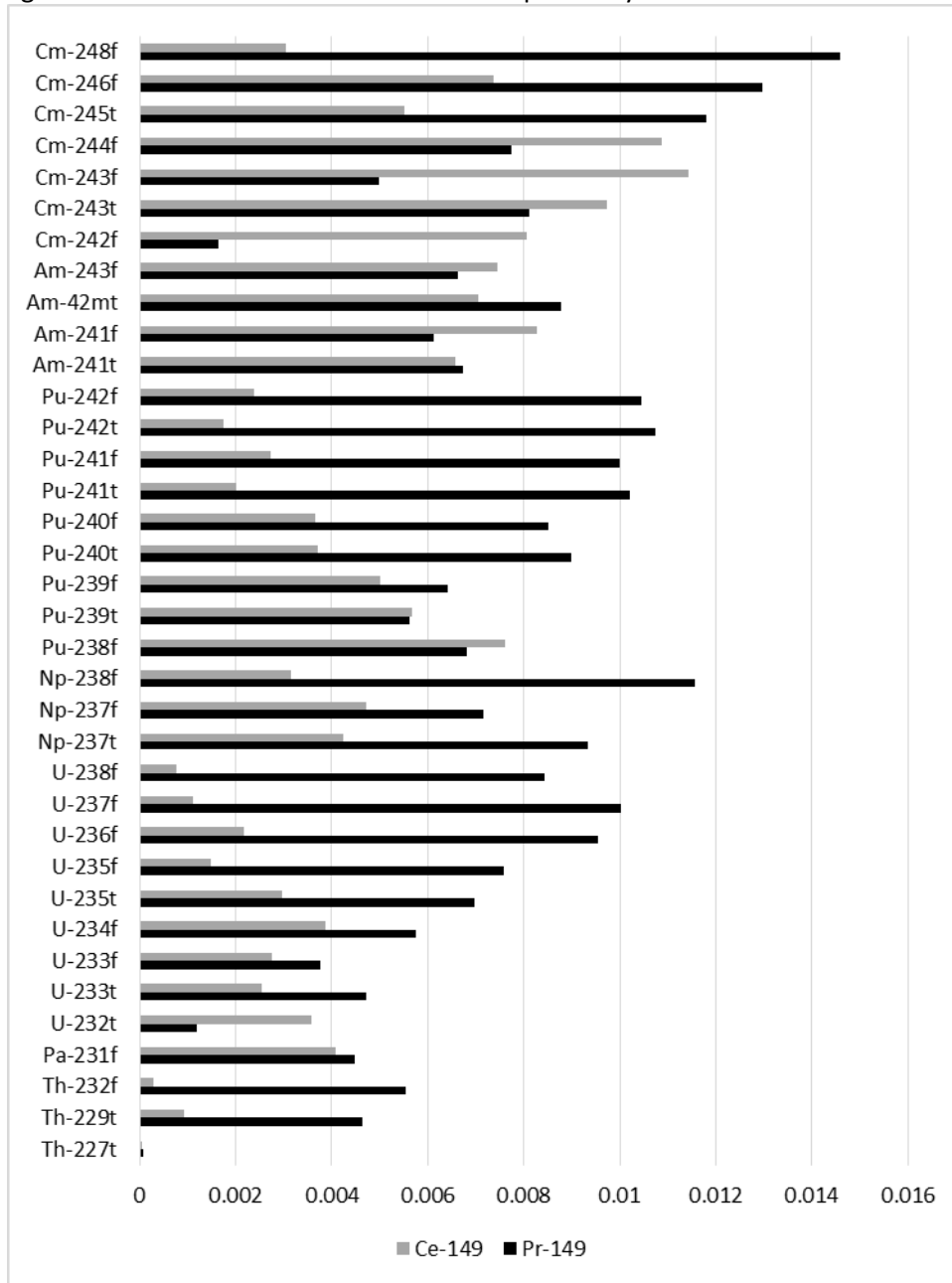
The authors believe these results show that the three methods have similar reactivity impacts; therefore the cumulated buildup of fission products from all actinides not explicitly containing a fission yield was not significant enough to alter the flux enough to further affect the buildup of nuclides in the H.B. Robinson benchmark. The major reactivity contributing fission products are Xe-135 (2.6E6 b thermal 1-group (n, γ)) and Sm-149 (40E3 b thermal 1-group (n, γ)). Figure 7 does show that the direct yields for Xe-135 from U-235, Pu-239, Pu-241 and Am-241 thermal fission and Pu-239 fast fission yield are slightly different; however, most Xe-135 is produced from I-135 and Te-135 beta decay, and the yields for I-135 and Te-135 are almost identical for all 5 targets. Figure 9 displays the thermal and fast fission yields for various actinides for Te-135 and I-135. The thermal yields of I-135 and Te-135 are reasonably close (same order of magnitude) for nearest element and isobar method. Sm-149 is produced by Ce-149 and Pr-149 beta decay. Figure 10 displays the thermal and fast fission yields for various actinides for Ce-149 and Pr-149. Except for the Cm isotopes, the yields of Ce-149 or Pr-149 for a particular actinide are relatively close for nearest element and isobar method. As a result of the yields being close for these major reactivity contributors, and the fact that minor actinide fission makes up less than 1% of the fissions occurring in the system, the flux shape was not significantly perturbed by the choice of fission yield method as the reactivity (i.e. competition for capture) contribution from Xe-135 and Sm-149 was not significantly different for each fission product yield method.

383 Figure 9. Selected thermal and fast fission product yields for Te-135 and I-135.



384
385
386

387 Figure 10. Selected thermal and fast fission product yields for Ce-149 and Pr-149.



388
 389
 390
 391
 392
 393
 394
 395
 396
 397
 398

Though no noticeable reactivity effect was realized from the difference in fission product buildup of the three methods, the fission product buildups of the three methods were still different. Comparing the percent difference of the isobar and element methods as compared to the base method, most fission products were within 7%. Table 10 displays the fission products, from MCNP6 fission product Tier 3, which contain larger than 7% relative difference as compared to the base method at 31.66 GWD/MTU. The yields of these fission products are not particularly large for U-235, U-238, Pu-239 or Pu-241 (which make up 99% of the fissions that occurred in the system).

399 Table 10. Percent difference in Tier 3 fission product buildup at 31.66 GWD/MTU for fission products
 400 containing larger than 7% relative difference as compared to the base method.

Isotope	Element Method	Isobar Method
Ga-69	-46.22	-0.46
Ga-71	-13.81	0.54
Pd-102	-7.24	1.54
Pd-105	-7.47	2.54
Pd-106	-7.53	3.54
Ag-109	-2.81	7.54
Cd-108	-2.82	8.54
Cd-110	-2.87	9.54
Cd-116	-7.34	10.54
Sn-115	-7.41	11.54
Sn-116	-7.86	12.54
Sn-117	-7.48	13.54
Sn-118	-11.77	14.54
Sn-119	-9.45	15.54
Sn-120	-9.76	16.54
Sn-122	-7.36	17.54
Sb-121	-8.29	18.54
Sb-123	-8.11	19.54
Te-122	-8.94	20.54
Te-123	-9.85	21.54
Te-124	-8.51	22.54
Er-166	-10.64	23.54
Er-167	-23.21	24.54
Er-168	-38.72	25.54

401

402

403 5. Conclusions

404

405 A significant approximation in any depletion solver is that the employed nuclear data is correct and
 406 complete. This study particularly focused on the treatment of fission yields for actinides not explicitly
 407 possessing fission yield data (specifically focusing on fission yields for the CINDER90 library file). Several
 408 types of approximations are used for estimating fission yields for actinides which do not possess explicit
 409 fission yield data. Based on examining fission yield data, three methods were tested for fission yield
 410 selection for actinides not possessing explicit fission yields: (1) the current CINDER90 library file method
 411 (Base); (2) the element method (Element); and (3) the isobar method (Isobar). The H. B. Robinson
 412 benchmark was used to assess the predictive capabilities of each method because of availability and
 413 simplicity of the model. Though this benchmark only contained major actinide data and 2 fission products,
 414 the benchmark does serve to assess the reactivity impact on major actinide and fission product prediction
 415 from minor actinide fission yield choice. Results do show that the three fission product selection methods
 416 result in similar reactivity contributions for this particular benchmark. The results are due to the product
 417 of the minor actinide fissions contributing less than 1% of total fissions and the fission yields of nuclides
 418 beta decaying to Xe-135 and Sm-149 being very similar for each selection method.

419

420 Several fission products do have production that is significantly different depending on the method for
 421 choosing a yield for actinides not possessing an explicit yield. Future applications may determine these

422 fission products to be useful in fuel characterization; however, an easily computable benchmark containing
423 these measured fission products will be required to assess the accuracy in prediction. To completely assess
424 the specific minor actinides responsible for differences in Table 10 requires a dissection of every fissioning
425 actinide in CINDER90, regardless of whether or not it is tracked in MCNP6, as well as a method of
426 determining how the transport is modified due to slight changes in fission product buildup. Though the
427 fission rates sent to CINDER90 are accessible for each actinide tracked in MCNP6, those actinides not
428 tracked in MCNP6 (those actinides that apply a 63-group MCNP flux to an 63-group cross section set in
429 CINDER90 internally) are not yet as accessible for the typical code user. Furthermore, estimating the
430 contribution, of a particular minor actinide to fission product differences in Table 10, by way of examining
431 the minor actinide fission rates sent to CINDER90, further requires weighting with the independent yields
432 of each fission product from each minor actinide. Nonetheless, to first order, choices for Pu-238, Np-238,
433 Np-239, Am-243, Cm-241, Cm-242 and Cm-244 are driving some of the differences seen in Table 10. Figure
434 7 also shows that independent yields can vary by several orders of magnitude. Therefore, if these fission
435 products are deemed important for future applications, future work should focus on the origin of their
436 difference for various fission product selection methods.

437

438 6. References

439

- 440 1. D. B. Pelowitz, editor, "MCNPX User's Manual Version 2.6.0," Los Alamos National Laboratory Report:
441 *LA-CP-07-1473*, Los Alamos, NM (2008).
- 442 2. W. B. WILSON, T. R. England, E. D. Arthur, C. A. Beard, C. D. Bowman, L. N. Engel, A. Gavron, D. C.
443 George. L. Daemen, H. G. Hughes, III, W. W. Kinnison, R. J. Labauve, D. M. Lee, H. Lichtenstein, P. W.
444 Lisowski, D.W. Muir, A. P. Muir, A. P. Palounek, R. T. Perry, E. J. Pitcher, R. E. Prael, R. J. Russel, G. Sanders,
445 L. S. Waters, P. G. Young and J. J. Ziock, "Accelerator Transmutation Studies at Los Alamos with LAHET,
446 MCNPX and CINDER90," *Proceedings of the Workshop on Simulation of Accelerator Radiation*
447 *Environments*, Santa Fe, NM (1993).
- 448 3. M. L. Fensin, J. S. Hendricks, S. Anghaie, "The Enhancements and Testing for the MCNPX 2.6.0
449 Depletion Capability," *Nuclear Technology*, **170**, Number 1, pp. 68-79 (2010).
- 450 4. T. Goorley, M. James, T. Booth, F. Brown, J. Bull, L.J. Cox, J. Durkee, J. Elson, M. Fensin, R.A. Forster, J.
451 Hendricks, H.G. Hughes, R. Johns, B. Kiedrowski, R. Martz, S. Mashnik, G. McKinney, D. Pelowitz, R.
452 Prael, J. Sweezy, L. Waters, T. Wilcox, T. Zukaitis, "Initial MCNP6 Release Overview: MCNP6 version
453 1.0," *Nuclear Technology*, **164**, Number 3, pp. 3-12 (2012).
- 454 5. M. L. Fensin, M. R. James, J. S. Hendricks, J. T. Goorley, "The New MCNPX Depletion Capability."
455 *International Congress on the Advancement in Nuclear Power Plants (ICAPP)*, Chicago, IL (2012).
- 456 6. R. J. J. Stamm'ler, M. J. Abbate, *Methods of Steady-State Reactor Physics in Nuclear Design*, Academic
457 Press, London (1983).
- 458 7. D. Kotlyar, E. Shwageraus, "On the use of predictor-corrector method for coupled Monte Carlo burnup
459 codes," *Annals of Nuclear Energy*, **58**, pp. 228-237 (2013).
- 460 8. A. Yamamoto, M. Tatsumi, N. Sugimura, Projected Predictor-Corrector Method for Burnup
461 Calculations of Gd-Bearing Fuel Assemblies," *American Nuclear Society Physics of Reactors*, Interlaken,
462 Switzerland (2008)
- 463 9. M. L. Fensin, J. S. Hendricks, S. Anhaie, "Incorporation of a predictor-corrector methodology and 1-
464 group reaction rate reporting scheme for the MCNPX depletion capability," *American Nuclear Society*
465 *Winter Meeting*, Albuquerque, New Mexico (2006)
- 466 10. M. Chadwick, P. Obložinský, M. Herman, N. Greene, R. McKnight, D. Smith, P. Young, R. MacFarlane, G.
467 Hale, S. Frankle, A. Kahler, T. Kawano, R. Little, D. Madland, P. Moller, R. Mosteller, P. Page, P. Talou, H.
468 Trelue, M. White, W. Wilson, R. Arcilla, C. Dunford, S. Mughabghab, B. Pritychenko, D. Rochman, A.
469 Sonzogni, C. Lubitz, T. Trumbull, J. Weinman, D. Brown, D. Cullen, D. Heinrichs, D. McNabb, H. Derrien,

470 M. Dunn, N. Larson, L. Leal, A. Carlson, R. Block, J. Briggs, E. Cheng, H. Huria, M. Zerkle, K. Koziar, A.
471 Courcelle, V. Pronyaev, S. van der Marck, "ENDF/B-VII. 0: Next generation evaluated nuclear data
472 library for nuclear science and technology," *Nuclear Data Sheets*, **107** (12), pp. 2931–3118 (2006)

473 11. A.J. Koning, M. Avrigeanu, V. Avrigeanu, P. Batistoni, E. Bauge, M.-M. Bé, P. Bem, D. Bernard, O.
474 Bersillon, A. Bidaud, O. Bouland, A. Courcelle, C.J. Dean, P. Dos-Santos-Uzarralde, B. Duchemin, I.
475 Duhamel, M.C. Duijvestijn, E. Dupont, U. Fischer, R.A. Forrest, F. Gunsing, W. Haeck, H. Henriksson, A.
476 Hogenbirk, T.D. Huynh, R. Jacqmin, C. Jouanne, J. Keinert, M.A. Kellett, I. Kodeli, J. Kopecky, H. Leeb,
477 D. Leichtle, J. Leppanen, O. Litaize, M.J. Lopez Jimenez, M. Mattes, E. Menapace, R.W. Mills, B.
478 Morillon, C. Mounier, A.L. Nichols, G. Noguere, C. Nordborg, A. Nouri, R.L. Perel, P. Pereslavtsev, R.J.
479 Perry, M. Pescarini, M. Pillon, A.J.M. Plompen, D. Ridikas, P. Romain, Y. Rugama, P. Rullhusen, C. de
480 Saint Jean, A. Santamarina, E. Sartori, K. Seidel, O. Serot, S. Simakov, J.-Ch. Sublet, S. Tagesen, A.
481 Trkov, S.C. van der Marck and H. Vonach, "The JEFF evaluated nuclear data project", *Proceedings of*
482 *the International Conference on Nuclear Data for Science and Technology*, Nice, France (2007)

483 12. K. Shibata, O. Iwamoto, T. Nakagawa, N. Iwamoto, A. Ichihara, S. Kunieda, S. Chiba, K. Furutaka, N.
484 Otuka, T. Ohsawa, T. Murata, H. Matsunobu, A. Zukeran, S. Kamada, and J. Katakura: "JENDL-4.0: A
485 New Library for Nuclear Science and Engineering," *Journal of Nuclear Science and Technology*, **48** (1),
486 pp. 1-30 (2011).

487 13. A.I. Blokhin, B.I. Fursov, A.V. Ignatyuk, V.N. Koshcheev, E.V. Kulikov, B.D. Kuzminov, V.N. Manokhin and
488 M.N. Nikolaev: "Current Status of Russian Evaluated Neutron Data Libraries," *Proc. of International*
489 *Conference on Nuclear Data for Science and Technology*, Gatlinburg, Tennessee (1994).

490 14. CHEN Guo-Chang, CAO Wen-Tian, YU Bao-Sheng, TANG Guo-You, SHI Zhao-Min, TAO Xi, "Neutron
491 nuclear data evaluation of actinide nuclei for CENDL-3.1," *Chinese Physics C*, **36** (9), pp. 823-826 (2012).

492 15. P. G. Young, E. D. Arthur, and M. B. Chadwick, "Comprehensive nuclear model calculations:
493 Introduction to the theory and use of the GNASH code," Los Alamos National Laboratory Report: LA-
494 12343-MS, Los Alamos, NM (1992).

495 16. M. Herman, R. Capote, B. V. Carlson, P. Obložinský, M. Sin, A. Trkov, H. Wienke, V. Zerkin, "EMPIRE:
496 Nuclear Reaction Model Code System for Data Evaluation," *Nuclear Data Sheets*, **108**, pp. 2655-2715
497 (2007).

498 17. Nuclear Data Section of the International Atomic Energy Agency "Compilation and evaluation of fission
499 yield nuclear data," International Atomic Energy Agency Document: IAEA-TECDOC-1168, Vienna,
500 Austria (2000).

501 18. A. G. CROFF, "ORIGEN2: A Versatile Computer Code for Calculating the Nuclide Compositions and
502 Characteristics of Nuclear Materials," *Journal of Nuclear Technology*, **62**, pp. 335-352 (1983).

503 19. I. C. Gauld , "Origen-S: Depletion Module to Calculate Neutron Activation, Actinide Transmutation,
504 Fission Product Generation, and Radioactive Source Terms," Oak Ridge National Laboratory Report:
505 ORNL/TM-2005/39, Oak Ridge, TN (2011).

506 20. I. C. Gauld and D. Wiarda, "ORIGEN-S Data Libraries," Oak Ridge National Laboratory Report:
507 ORNL/TM-2005/39, Oak Ridge, TN (2011).

508 21. A. Tsilanizara, S. Lahaye, E. Brun, Etat du solveur Evolution et les premières vérifications, CEA SACLAY
509 Report: SERMA/LLPR/RT/09-4640/A, Cedex, France (2009).

510 22. Ding She, Kan Wang, Ganglin Yu, "Development of the point-depletion code DEPTH," *Nuclear*
511 *Engineering and Design*, **258**, pp. 235– 240 (2013) .

512 23. A.E. Isotalo, P.A. Aarnio, "Comparison of depletion algorithms for large systems of nuclides," *Annals of*
513 *Nuclear Energy*, **38**, pp. 261-268 (2011).

514 24. O. W. Hermann, S. M. Bowman, M. C. Brady, C. V. Parks, "Validation of the SCALE System for PWR Spent
515 Fuel Isotopic Composition Analysis," Oak Ridge National Laboratory Report: ORNL/TM-12667, Oak
516 Ridge, TN, USA (1995).

517 25. Forrest B. Brown, "The maksf Code with Doppler Broadening," Los Alamos National Laboratory
518 Report: LA-UR-06-7002, Los Alamos, NM (2006).
519